Mineralogical Magazine, November 2015, Vol. 79(6), pp. 1529–1542

OPEN ACCESS

The initial dissolution rates of simulated UK Magnox–ThORP blend nuclear waste glass as a function of pH, temperature and waste loading

N. Cassingham[1], C.L. Corkhill[1,*], D.J. Backhouse[1], R.J. Hand[1], J.V. Ryan[2], J.D. Vienna[2] and N.C. Hyatt[1,*]

[1] Immobilisation Science Laboratory, Department of Materials Science and Engineering, The University of Sheffield, UK

[2] Energy and Environment Directorate, Pacific Northwest National Laboratory, Richland, Washington, USA

[*Received 30 September 2014; Revised 1 June 2015; Associate Editor: Nick Evans*]

ABSTRACT

The first comprehensive assessment of the dissolution kinetics of simulant Magnox–ThORP blended UK high-level waste glass, obtained by performing a range of single-pass flow-through experiments, is reported here. Inherent forward rates of glass dissolution were determined over a temperature range of 23 to 70°C and an alkaline pH range of 8.0 to 12.0. Linear regression techniques were applied to the TST kinetic rate law to obtain fundamental parameters necessary to model the dissolution kinetics of UK high-level waste glass (the activation energy (E_a), pH power law coefficient (η) and the intrinsic rate constant (k_0)), which is of importance to the post-closure safety case for the geological disposal of vitreous products. The activation energies based on B release ranged from 55 ± 3 to 83 ± 9 kJ mol^{-1}, indicating that Magnox–THORP blend glass dissolution has a surface-controlled mechanism, similar to that of other high-level waste simulant glass compositions such as the French SON68 and LAW in the US. Forward dissolution rates, based on Si, B and Na release, suggested that the dissolution mechanism under dilute conditions, and pH and temperature ranges of this study, was not sensitive to composition as defined by HLW-incorporation rate.

Keywords: glass, dissolution mechanism, geological disposal.

Introduction

To predict the performance of nuclear waste glasses in a geological disposal facility (GDF), an understanding of the glass dissolution rate, in the context of the geochemical settings, is required. In recent years, several studies have focused on understanding the mechanism of glass alteration (for a recent overview, see Gin *et al.*, 2013*a*, and references therein) as a function of composition, temperature, pH and solution chemistry; e.g. French SON68 glass (Curti *et al.*, 2006; Gin *et al.*, 2013*b*) and USA LAW glasses (e.g. McGrail *et al.*, 1997; Pierce *et al.*, 2008). The kinetics of glass dissolution are typically modelled using Transition State Theory (TST), which, in its simplified form, is given by:

$$R_i = k_0 v_i e^{-E_a/RT} a_{H^+}^{\eta} \left[1 - \left(\frac{Q}{K}\right)^{\sigma}\right] \qquad (1)$$

where R_i is the release rate of glass component i, k_0 is the intrinsic rate constant, v_i is the stoichiometric coefficient for element i, E_a is the activation energy,

* E-mail: c.corkhill@sheffield.ac.uk; n.c.hyatt@sheffield.ac.uk

DOI: 10.1180/minmag.2015.079.6.28

The publication of this research has been funded by the European Union's European Atomic Energy Community's (Euratom) Seventh Framework programme FP7 (2007–2013) under grant agreements n°249396, SecIGD, and n°323260, SecIGD2.

R*T* is the product of the gas constant and the absolute temperature, a_{H+} is the hydronium ion activity, η^{H+} is the reaction order with respect to a_{H+}, *Q* is the activity product of the rate-limiting reaction, K is the equilibrium constant for the reaction, and σ is the overall reaction order (McGrail *et al.*, 1997). Several different experimental methods have been applied to determine glass-dissolution behaviour; conventional static PCT and MCC-1 methods are most widely applied (ASTM, 1994; MCC, 1981). Flow-through approaches, including single-pass flow-through (SPFT) and micro-channel flow-through (MCFT) methodologies, however, are considered most appropriate to determine the reaction kinetics of glass dissolution (McGrail and Peeler, 1995). The continual introduction of fresh reaction media in the 'flow-through' methodology ensures that conditions are dilute, which is necessary to prevent the accumulation of reaction products. This maintains the chemical affinity term, *Q*/K, at near zero so that the inherent 'forward rate' of dissolution is sustained and experimental parameters such as temperature and pH can be varied to yield an accurate quantitative description of their impact on dissolution kinetics.

In the UK, the high-level waste (HLW) calcine resulting from Magnox and ThORP (Thermal Oxide Reprocessing Plant) reprocessing operations is combined in a ~1:3 ratio (Magnox:ThORP calcine) and vitrified in a borosilicate glass. Waste loadings of this vitrified product have typically been in the range of 25–28 wt.% (on the basis of metal oxides), although increased waste loadings have been demonstrated and produced successfully (Harrison *et al.*, 2012). In comparison, the waste loading of a similar French product is typically 15–18 wt.% (Curti *et al.*, 2006). To date, studies of the mechanism and kinetics of the dissolution of non-radioactive analogues of this complex glass blend have been limited to static batch experiments. For example, Corkhill *et al.* (2013) determined the leaching mechanisms of monolith samples for 168 days in water; Hyatt *et al.* (2004) performed an evaluation of the dissolution behaviour under the likely conditions of very deep borehole geological disposal and Utton *et al.* (2012) and Corkhill *et al.* (2013) investigated the static dissolution behaviour in simulated cement pore waters. The dissolution kinetics of inactive simulant Magnox glass have also received limited attention; a small matrix of static experiments and flow-through experiments at 40°C and pH 10 were performed by Abraitis *et al.* (2000*a,b,c*), while Curti *et al.* (2006) performed long-term (548 days) leaching experiments on Magnox glass powder at 90°C in distilled water and showed that SON68 is approximately seven times more durable than Magnox glass. Note, however, that HLW glasses produced from a pure Magnox waste composition will ultimately form a small fraction of the total 2900 tonnes of vitrified product destined for geological disposal (NDA, 2014); the majority of the inventory will be of a blend composition. Consequently, it is imperative to understand the mechanism and to quantify the kinetics of Magnox–ThORP blend glass.

This investigation utilizes the single-pass flow-through methodology in order to provide the first comprehensive study of the dissolution kinetics of simulant UK Magnox–ThORP blended HLW glass. Furthermore, because it is important from an economic and operational perspective to maximize the waste loading of the vitrified HLW product, we investigate the effect of increasing the percentage of the Magnox component of the blend glass on the forward rate of dissolution.

Experimental procedure

Glass synthesis

Simulant Magnox–ThORP blend glasses (blended at a ratio of 1:3) were prepared at two different waste loadings: 25 wt.% (referred to as MT25 throughout the investigation) and 30 wt.% (referred to as MT30 throughout the investigation). Glasses were prepared using a baseline glass frit and a blended nuclear waste simulant calcine, both kindly provided by the National Nuclear Laboratory, UK. Batched frit and calcine were mixed by hand in HDPE bottles for 2 min, added to a pre-heated mullite crucible and placed in a furnace at 1060°C for 1 h. Subsequently, the batch was stirred for a further 4 h at 1060°C, cast into a block using a pre-heated stainless steel mould, annealed at 500°C for 1 h, and then cooled at 1°C min^{-1} to room temperature. Final glass compositions, as measured using X-ray fluorescence (Assay Office, Sheffield, UK) are given in Table 1. X-ray diffraction and SEM/EDX analysis confirmed the homogeneous nature of the glass compositions formed.

Glasses were crushed and powdered using a Tema ring and puck mill and sieved to the 75–150 μm size fraction, giving an average glass-particle radius of 56.3 ± 0.65 μm. Density measurements of both glasses were performed using the Archimedes method yielding a density of 2.77 ± 0.01 g cm^{-2}. The surface area of the glass powders was calculated

TABLE 1. Chemical compositions (wt.%) of simulant Magnox – ThORP blend nuclear waste glass specimens.

Oxide component	MT25	MT30
SiO_2	46.28	44.33
B_2O_3	18.3	17.74
Na_2O	8.12	7.74
Li_2O	4.81	4.34
Gd_2O_3	3.86	4.17
ZrO_2	2.40	2.81
MoO_3	2.02	2.48
Al_2O_3	1.87	2.35
Fe_2O_3	1.87	2.06
Nd_2O_3	1.81	1.86
Cs_2O	1.61	1.99
MgO	1.34	1.64
CeO_2	1.24	1.38
BaO	1.22	1.38
La_2O_3	0.67	0.73
RuO_2	0.49	0.51
Pr_2O_3	0.47	0.46
Cr_2O_3	0.37	0.46
SrO	0.32	0.36
NiO	0.28	0.47
Sm_2O_3	0.28	0.33
TeO_2	0.28	0.30
Y_2O_3	0.10	0.10
Total	100.00	99.99

geometrically, according to Icenhower and Steefel (2013). Glass powders were cleaned prior to dissolution according to the Product Consistency Test (PCT) ASTM standard (ASTM, 1994).

Buffer solutions

The buffer solutions used to control the pH during single-pass flow-through experiments are summarized in Table 2. For buffer solutions at pH 8.0 and 10.0, measured amounts of the organic tris hydroxymethyl aminomethane buffer (THAM, 99% purity, Fisher Scientific) were added to ultra-high quality (18 MΩ cm^{-1}) water and adjusted to the desired pH at room temperature (23 ± 2°C) with 15 M HNO_3 (99.999% trace metals basis, Fisher Scientific). Final pH values at room temperature [denoted throughout the study as pH(23°C)] were pH(23°C) 8.00 ± 0.05 and pH(23°C) 10.00 ± 0.05. For buffer solutions at pH 12.0, 0.01 M LiOH and 0.01 M LiCl (both 99.99% purity, Alpha Aesar) were prepared and adjusted to pH(23°C) 12.00 ± 0.05 with 0.01 M LiOH. To ensure the accuracy of the buffered pH value, especially under the highest pH conditions, which may be susceptible to pH drift, the solution pH was measured under the desired test conditions at regular time points for 48 h. No drift in pH values was observed (within error), indicating that atmospheric CO_2 did not lower the pH for the duration of the SPFT experiments. Table 2 gives a summary of the pH values calculated for each test temperature (23°C, 40°C and 70°C) using the *PHREEQC* geochemical modelling software with the LLNL database.

Single-pass flow-through methodology

All single-pass flow-through (SPFT) experiments utilized Kloehn v6 syringe pumps. Buffer solutions were transferred from 1 L HDPE input reservoirs to PTFE reactors *via* PTFE tubing into one of two ports on the vessel lid. The buffer solutions and reaction vessels were both kept in a constant-temperature oven (±2°C) in order to minimize the effects of varying temperature between the buffer solution reservoir and the reaction vessel. The solution was then transferred from the second port in the reaction vessel, via PTFE tubing, to an HDPE

TABLE 2. Chemical compositions of buffer solutions used for single-pass flow-through experiments. Solution pH values (±0.05 pH units) above 23°C were calculated using PHREEQC (LLNL database).

Solution	Composition	pH		
		23°C	40°C	70°C
1	0.05 M THAM* + 15 M HNO_3 pH adjustment	8.0	7.9	7.6
2	0.05 M THAM + 15 M HNO_3 pH adjustment	10.0	9.8	9.3
3	0.01 M LiOH + 0.01 M LiCl pH adjustment	12.0	11.5	10.7

*THAM = tris hydroxymethyl aminomethane buffer.

collection vessel outside the oven, prior to analysis. The flow rate was determined by weighing the volume of solution collected at each sampling time; variations were typically <3%. Once constant conditions were established (e.g. buffer pH, temperature of blank solution and flow rate), crushed glass was placed within each test vessel. Experiments were run at flow rates ranging from 5 ml d^{-1} to 125 ml d^{-1} until steady-state effluent chemistries were observed. Blank experiments were performed in order to provide controlled blank analyses. All effluent solutions were analysed for Si, B and Na using inductively coupled plasma optical emission spectroscopy (ICP-OES) and pH was measured using a calibrated pH electrode. Due to the dilute conditions of the experiments, it was only possible to measure those elements that are present in the solution above the detection limit, therefore it was not possible to present data for the minor elements in each glass composition (the detection limits for the major elements analysed, B, Si and Na, were 10, 20 and 50 μg l^{-1}, respectively). For a detailed account of the SPFT apparatus, the reader is directed to the extensive descriptions by McGrail *et al.* (1997), Pierce *et al.* (2005, 2008), Icenhower *et al.* (2006) and Wellman *et al.* (2006).

Quantification of dissolution rates

Normalized elemental release rates were determined by equation 2:

$$R_i = \frac{(C_i - \bar{C}_{i,b})q}{f_i S} \quad (2)$$

where R_i is the normalized glass dissolution rate of element i (g m^{-2} d^{-1}), C_i the concentration of element i in the effluent (g l^{-1}), $\bar{C}_{i,b}$ the average background concentration of element i (g l^{-1}), q the flow-through rate (l d^{-1}), f_i the mass fraction of the element in the glass (unitless), and S the surface area of the sample (m^2). Determination of the experimental uncertainty of the dissolution rate considered the uncertainties of each parameter described in equation 2. For uncorrelated random errors, the standard deviation of a function f(x_1, x_2, x_n) is given by:

$$\sigma_f = \sqrt{\sum_{i=1}^{n} \left(\frac{\partial f}{\partial x_i}\right)^2 \sigma_i^2} \quad (3)$$

where σ_f is the standard deviation of the function f, x_i the parameter i, and σ_i the standard deviation of parameter i. Substituting equation 2 into equation 3 and converting to relative errors, $\hat{\sigma}_{ri} = \sigma_{R_i}/R_i$, gives:

$$\hat{\sigma}_{Ri} = \sqrt{\frac{(\hat{\sigma}_{Ci}C_i)^2 + (\hat{\sigma}_{\bar{C}i,b}\bar{C}_{i,b})^2}{(C_i - \bar{C}_{i,b})^2} + \breve{\sigma}_q^2 + \breve{\sigma}_{fi}^2 + \breve{\sigma}_S^2} \quad (4)$$

relative errors of $\hat{\sigma}_{Ci}$, $\hat{\sigma}_{\bar{C}i}$, $\hat{\sigma}_q$, $\hat{\sigma}_{fi}$, and $\hat{\sigma}_S$ are 10%, 10%, 5%, 3% and 15%, respectively (Pierce *et al.*, 2010).

Results and Discussion

Effect of flow rate (q) to sample surface area (S) ratio on dissolution rate

Prior to performing experiments to determine the dependence of dissolution rate on temperature and pH, the effect of varying the ratio of flow rate, q, to sample surface area, S, was determined experimentally by altering the flow rate or the mass of the glass sample used in an SPFT experiment. Varying the q/S ratio can influence the chemical potential between the glass and a solution; at low q/S values the concentration of elements dissolved in solution from the glass is high; conversely at high q/S values, the concentration of elements dissolved in solution is low, thereby minimizing the effect of chemical potential on dissolution. The desired q/S value is relatively high, ensuring that the dissolution is independent of q/S, such that the forward rate of dissolution is acquired.

The variation of q/S was investigated at 40°C and pH(23°C) = 8.0. The normalized dissolution rates based on the concentrations of Si, B and Na as a function of q/S are shown for the MT25 (Fig. 1*a*) and MT30 (Fig. 1*b*) glass blends. For MT25, the normalized dissolution rates of the elemental components were found to reach a constant value of $R_B = 0.049 \pm 0.006$ g m^{-2} d^{-1} at $\log_{10}(q/S) \approx -7.5$ m s^{-1} (Fig. 1*a*). For the MT30 glass, shown in Fig, 1*b*, a constant value of $R_B = 0.020 \pm 0.001$ g m^{-2} d^{-1} was achieved at $\log_{10}(q/S) \approx -7.5$ m s^{-1}. For both glass compositions, $\log_{10}(q/S)$ values of –6.8 to –9.2 m s^{-1} were attempted; variations from set flow rates were observed at low q/S values, however, between $\log_{10}(q/S)$ values of –9.2 and –8.0 m s^{-1} for MT25, and $\log_{10}(q/S)$ values of –9.2 and –8.3 m s^{-1} for MT30. This deviation was due to air becoming trapped within the tubing that transfers effluent from the reaction vessel to the collection vessel. Previous SPFT investigation of Magnox glass found that the normalized

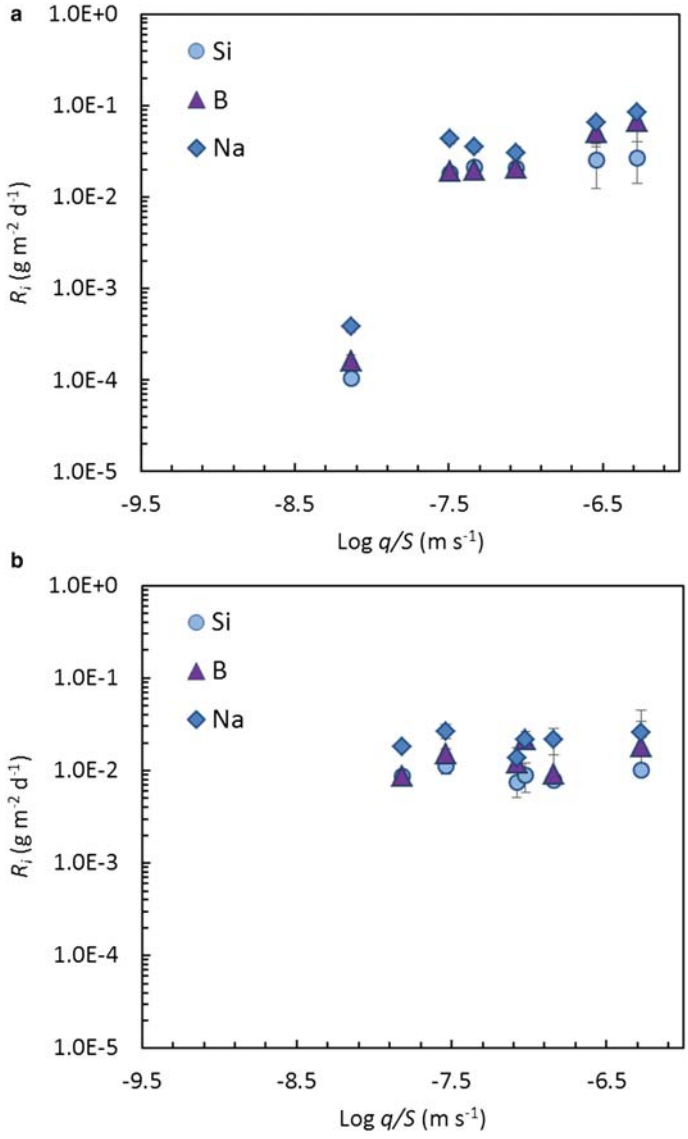

FIG. 1. Normalized dissolution rate (NR_i, g m^{-2} d^{-1}) as a function of flow rate (q) to sample surface area (S), (m s^{-1}), for Si, B and Na at T = 40°C and pH(23°C) = 8.0 for (*a*) MT25 and (*b*) MT30 blend simulated waste glass.

dissolution rate of B and Si became constant, i.e. independent of q/S, at a $\log_{10}$ (q/S) value of –6.3 m s^{-1} at 40°C and pH(23°C) = 10.0 (Abraitis *et al.*, 2000*b*). Similarly, in their study of simulated vitrified Hanford Low Activity Waste (LAW), McGrail *et al.* (1997) reported that Na and Si dissolution rates became independent of q/S at a $\log_{10}$ (q/S) value of –7.3 m s^{-1} at 40°C and pH(23°C) = 9.0. As such, although it was not possible to report the full range of $\log_{10}$ (q/S) values due to experimental issues, we are confident that the selection of a $\log_{10}$ (q/S) value of > –7.5 m s^{-1} is suitable for analysis of a q/S independent dissolution rate. Furthermore, as it is understood that using the highest possible q/S value eliminates the potential effects of temperature increase on the dissolution rate (McGrail *et al.*, 1997), a $\log_{10}$ (q/S) value of –6.5 ± 10% m s^{-1} was

selected to determine the forward rate of dissolution for both MT25 and MT30 blend glasses. Figure 1 also illustrates that over the range of *q/S* values investigated, the constituent elements Si, B and Na were released congruently from both glass compositions, within experimental error. This further confirms the appropriate choice of a higher $\log_{10}$ (*q/S*) value.

Effect of temperature on dissolution rate

Experiments were performed at a range of temperatures (23°C, 40°C and 70°C) to evaluate the effect of temperature on the rate of MT25 and MT30 blend glass dissolution. The normalized dissolution rates for Si, B and Na as a function of temperature at three different pH(23°C) values are given in Table 3 and Fig. 2.

The normalized dissolution rates of MT25 and MT30 blend glass compositions are comparable with those for Magnox glass studied under SPFT conditions. For example, Abraitis *et al.* (2000*b*), who reported rates based on B release only, observed a dissolution rate, R_B, of 0.139 ± 0.034 g m^{-2} d^{-1} at 40°C and pH 10, compared with an R_B of 0.106 ± 0.032 g m^{-2} d^{-1} for MT25 under the same conditions in the current study (Table 3). The similarity of the B release rates reported here to those of Abraitis *et al.* (2000*b*)

TABLE 3. Normalized dissolution rate (g m^{-2} d^{-1}) of Si (R_{Si}), B (R_B) and Na (R_{Na}) and for MT25 and MT30 blend simulated waste glass as a function of pH and temperature, including the difference in normalized dissolution rate (ΔR_i) between the two compositions.

pH	Temperature (°C)	MT25 R_i (g m^{-2} d^{-1})	MT30 R_i (g m^{-2} d^{-1})	ΔR_i (g m^{-2} d^{-1})
R_{Si}				
8	23	0.011 ± 0.004	0.020 ± 0.001	0.009
8	40	0.119 ± 0.036	0.105 ± 0.032	0.014
8	70	0.945 ± 0.284	0.369 ± 0.091	0.576
10	23	0.027 ± 0.010	0.024 ± 0.009	0.003
10	40	0.321 ± 0.096	0.436 ± 0.143	0.115
10	70	4.148 ± 1.245	6.038 ± 3.156	2.890
12	23	0.642 ± 0.249	0.778 ± 0.217	0.136
12	40	4.403 ± 1.323	7.638 ± 3.156	3.235
12	70	45.786 ± 6.767	61.292 ± 9.016	15.506
R_B				
8	23	0.005 ± 0.001	0.005 ± 0.002	0.000
8	40	0.051 ± 0.015	0.022 ± 0.003	0.029
8	70	0.395 ± 0.119	0.369 ± 0.091	0.026
10	23	0.027 ± 0.010	0.024 ± 0.003	0.003
10	40	0.106 ± 0.032	0.189 ± 0.080	0.083
10	70	2.548 ± 0.772	1.570 ± 0.471	0.978
12	23	0.489 ± 0.189	0.536 ± 0.208	0.047
12	40	2.160 ± 0.651	2.643 ± 0.401	0.483
12	70	12.059 ± 5.220	4.915 ± 1.480	7.144
R_{Na}				
8	23	0.011 ± 0.001	0.015 ± 0.004	0.004
8	40	0.057 ± 0.022	0.050 ± 0.019	0.006
8	70	1.006 ± 0.305	0.497 ± 0.497	0.509
10	23	0.010 ± 0.030	0.067 ± 0.022	0.034
10	40	0.225 ± 0.068	0.394 ± 0.167	0.169
10	70	4.827 ± 2.064	5.684 ± 0.859	0.857
12	23	1.963 ± 0.760	0.899 ± 0.221	0.164
12	40	6.827 ± 2.064	3.146 ± 1.335	3.681
12	70	33.049 ± 5.749	18.763 ± 5.647	14.286

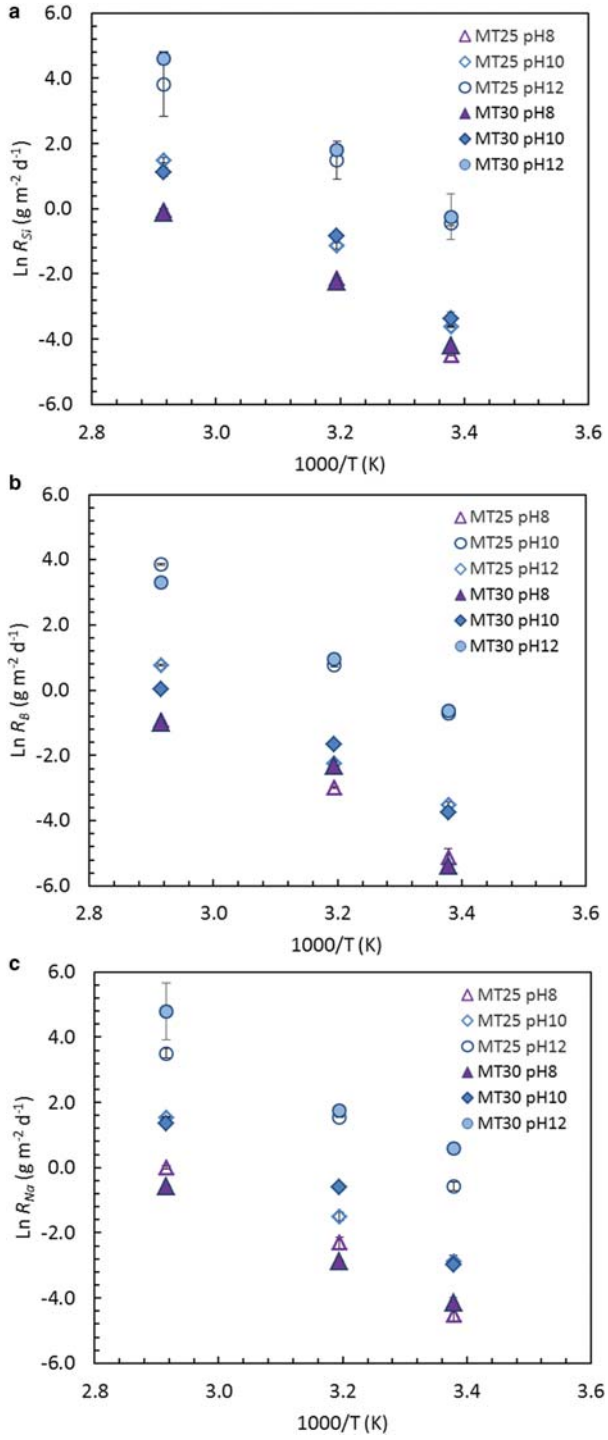

FIG. 2. Ln normalized dissolution rate (R_i, g m^{-2} d^{-1}) as a function of the inverse of temperature (from 23 to 70°C) and pH (23°C) of 8.0, 10.0 and 12.0 of: (*a*) Si; (*b*) B; and (*c*) Na, for MT25 and MT30 blend simulated waste glass.

suggest that the dependence of dissolution on glass composition is weak in the case of Magnox and Magnox–ThORP blend glass; it is not possible, however, to confirm this observation without additional comparison of Si and Na release rates under the full range of conditions investigated.

Dissolution rates for Magnox glass and Magnox–ThORP blend glass obtained through conventional static leaching methods at pH(23°C) = ~10 show a high degree of variability in the dissolution rate. For example, Utton *et al.* (2012) reported an R_B of 0.024 ± 0.004 g m^{-2} d^{-1} for MT25 blend glass powders at pH(23°C) = ~10.0 for 89 days (a factor of two greater than reported in the current study) while Curti *et al.* (2006) reported a significantly lower value of R_B ($9.6 \pm 5.3 \times 10^{-4}$ g m^{-2} d^{-1}) for Magnox simulant glass powders leached at pH 9.6 for 548 days; the lower value may reflect the potentially passivating nature of the alteration products formed on the glass surface. Interestingly, although alteration layers were also formed on the surface of monolith MT25 blend glass samples leached in water for 168 days at pH(23°C) = ~10.0, Corkhill *et al.* (2013) reported an R_B of 0.030 ± 0.003 g m^{-2} d^{-1}, similar to that reported for the forward rate under the same conditions in the current study. This variability is probably due to the methodology employed; as discussed previously, static experiments are subject to solution feedback effects, i.e. the accumulation of reaction products, which influences the dissolution rate. These results highlight the importance of using flow-through methodologies to accurately, and reproducibly, determine the dissolution kinetics of high-level waste glasses under conditions relevant to geological disposal.

The results in Table 3 show that increasing the temperature resulted in an increase in the normalized dissolution rate of each element. The observed dependence of temperature on the dissolution rate can be described by the Arrhenius equation:

$$r = A^{\frac{-E_a}{RT}} \quad (5)$$

where r is the dissolution rate (g m^{-2} d^{-1}), A is the Arrhenius parameter (g m^{-2} d^{-1}), E_a is the activation energy (kJ mol^{-1}), R is the ideal gas constant in J (mol K)$^{-1}$ and T is the temperature (K). Using the Arrhenius dependence of dissolution rate on temperature, linear regression of the data plotted in Fig. 2 was used to calculate the activation energy for Si, B and Na at each pH value, in both MT25 and MT30 blend glass compositions. The resulting values and 2σ errors are shown in Table 4. The E_a values for both glass blends were found to range between 67.5 ± 0.9 and 96.4 ± 28.8 kJ mol^{-1} for Si, 55.1 ± 3.2 and 83.1 ± 9.1 kJ mol^{-1} for B and between 52.2 ± 2.8 and 84.2 ± 9.2 kJ mol^{-1} for Na. These values are comparable to activation energy values for Magnox glass ($E_a = 56$ to 74 kJ mol^{-1}, Abraitis *et al.*, 2000*a*); pure silica ($E_a = 74.5$ kJ mol^{-1}, Dove, 1994; Icenhower and Dove, 2000), Hanford HAW glass ($E_a =$ 74.8 kJ mol^{-1}, McGrail *et al.*, 1997) and a number of other glass compositions in the aluminoborosilicate glass family (e.g. Wolff–Boesnich *et al.*, 2004; Pierce *et al.*, 2008, 2010; Jollivet *et al.*, 2012).

Within the limits of precision, the activation energy values for the MT25 and MT30 blend glasses are in the range proposed by Lasaga (1981) to be consistent with a surface–controlled dissolution mechanism (typically from 41 and 84 kJ mol^{-1}). This mechanism is widely agreed to occur by the inter-diffusion between H (as H^+ or H_3O^+) in solution and network modifying cations in the glass, whilst ionic–covalent bonds of the network forming elements (Si–O–Si, Si–O–B, Si–O–Na, etc.) undergo hydrolysis, resulting in nucleophilic attack by OH^- (Gin *et al.*, 2013*a*). The rate-limiting

TABLE 4. Calculated activation energies ($E_{a(i)}$, kJ mol^{-1}) for MT25 and MT30 blend simulated waste glass, derived from regression analysis based on the steady-state release of Si, B and Na, including the difference in $E_{a(i)}$ between the two glass blend compositions.

pH	$E_{a(Si)}$ (kJ mol^{-1})			$E_{a(B)}$ (kJ mol^{-1})			$E_{a(Na)}$ (kJ mol^{-1})		
	MT25	MT30	$\Delta E_{a(Si)}$	MT25	MT30	$\Delta E_{a(B)}$	MT25	MT30	$\Delta E_{a(Na)}$
8	78.1 ± 5.9	67.5 ± 0.9	10.6	55.1 ± 3.2	57.9 ± 2.4	2.8	58.4 ± 4.8	52.2 ± 2.8	6.2
10	90.5 ± 5.7	85.4 ± 0.3	5.1	79.7 ± 9.6	66.1 ± 3.2	13.6	80.4 ± 7.5	77.3 ± 10.9	3.1
12	96.4 ± 28.8	86.2 ± 20.2	8.4	83.1 ± 9.1	70.8 ± 2.0	12.3	84.2 ± 9.2	76.6 ± 8.1	7.6

step in this reaction is considered to be the rupture of Si–O bonds and detachment of Si (Lasaga, 1995; Icenhower *et al.*, 2008). Our results support this hypothesis; the activation energy for Si in both glass compositions was found to be higher than that for B and Na (Table 4), indicating that the rate-limiting step of the dissolution mechanism is the release of Si into solution.

Effect of solution pH on dissolution rate

Experiments were performed at a range of alkaline pH(23°C) values, from 8.0 to 12.0. These alkaline values were chosen for investigation for several reasons: firstly, under slow groundwater-flow conditions the repository environment is expected to buffer to slightly alkaline pH, for example, bentonite is predicted to buffer groundwater to a pH between 7.0 and 10.5 (Marsal *et al.*, 2007); secondly, although UK HLW vaults will probably be backfilled with clay, the potential interaction of alkaline solutions from concrete vault structures with vitrified HLW cannot be precluded on the timescales of GDF operation (10^5–10^6 y); and finally, the potential co-location of vitrified UK HLW with cementitious UK intermediate level waste may lead to the interaction of vitrified products with a high-pH groundwater derived from interaction with cementitious waste and backfill in the long term.

Figure 3 shows the $\log_{10}$ dissolution rates for Si, B and Na (Figs 3*a–c*, respectively) as a function of pH(23°C) at 23°C, 40°C and 70°C. The normalized dissolution-rate data are also given in Table 3. The dissolution rates were shown to increase with increasing pH for all of the components within each blend glass composition, e.g. for MT25 at 23°C, the R_B increased from 0.020 ± 0.005 at pH(23°C) = 8.0, to 0.027 ± 0.010 at pH(23°C) = 10.0, and to 12.059 ± 5.220 at pH(23°C) = 12.0. Interestingly, the dissolution rates derived from boron release were consistently lower than those derived from Na or Si, especially at higher pH values (Table 3). In their molecular-dynamics investigation of the hydrolysis of Na-borosilicate glass surfaces, Zapol *et al.* (2013) found B–O–B and B–O–Si bridges were likely to be more stable at high pH compared with Si–O–Si bridges, which may explain the incongruent dissolution observed here for Si and B. A similar effect was observed experimentally by Pierce *et al.* (2008), who concluded that this reflected an increased rate of alkali ion exchange at high pH, associated with the breakdown of silanol bonds at the surface, which in effect 'masked' the matrix dissolution and resulted in a reduced B release rate. The solubility of silica above pH 9 is known to dramatically increase due to the dissociation of H_3SiO_4 into $H_3SiO_4^-$ and $H_2SiO_4^{2-}$ species. As a consequence, it may be expected that the rate of Si release, and hence alkali ion release through ion exchange processes, above pH 9 is increased and the glass network, particularly at the surface, begins to break down. The behaviour of the two UK blend glasses investigated in this study appears consistent with this general mechanism.

A linear regression of the $\log_{10}$ normalized dissolution rates of Si, B and Na shown in Fig. 3 was performed using equation 6 to calculate the pH power-law coefficient (e.g. order of reaction), η (dimensionless), and intrinsic rate constant, k_0 (g m^{-2} d^{-1}), for the MT25 and MT30 blend glasses at each of the temperatures investigated. The results are shown in Tables 5 and 6, respectively.

$$R = k_0 10^{\eta[pH]} \quad (6)$$

The η values reported for MT25 and MT30 are similar, and are in the range of $\eta_{Si} = 0.39 \pm 0.02$ to 0.49 ± 0.02, $\eta_B = 0.33 \pm 0.02$ to 0.53 ± 0.03, and $\eta_{Na} = 0.42 \pm 0.02$ to 0.58 ± 0.03 (Table 5). These values are similar to those reported for other glass materials, e.g. Magnox glass ($\eta_B = 0.43 \pm 0.07$, Abraitis *et al.*, 2000*a*); R7T7 ($\eta_B = 0.39$, Vernaz and Dussossoy, 1992); basaltic and pure silica glass ($\eta_{Si} = 0.40$, Brady and House, 1996) and other glasses in the aluminoborosilicate family, e.g. $\eta_{Si} = 0.40 \pm 0.03$ (McGrail *et al.*, 1997), $\eta_B = 0.40 \pm 0.04$ (Pierce *et al.*, 2008) and $\eta_{Na} = 0.45 \pm 0.14$ (Pierce *et al.*, 2010).

The intrinsic rate constants for each element, calculated using a linear regression of data in Fig. 3 according to equation 6, were found to increase with increasing temperature (Table 6). For MT25, k_{Si} was found to be $(2.84 \pm 0.31) \times 10^{-6}$ g m^{-2} d^{-1} at 23°C and $(4.68 \pm 0.52) \times 10^{-4}$ g m^{-2} d^{-1} at 70°C. This is in agreement with observations of LAW simulant glass dissolution, e.g. Pierce *et al.* (2008) reported values for k_{Si} of $(8.30 \pm 7.00) \times 10^{-7}$ g m^{-2} d^{-1} at pH(23°C) and $(4.74 \pm 2.09) \times 10^{-5}$ g m^{-2} d^{-1}at pH(70°C). Values of k_B and k_{Na} also increased with increasing temperature, although to a lesser extent than observed for k_{Si}, consistent with the greater activation energies derived for Si than B and Na (Table 4), and due to the participation of Si in the rate limiting step of the surface-controlled dissolution mechanism. It

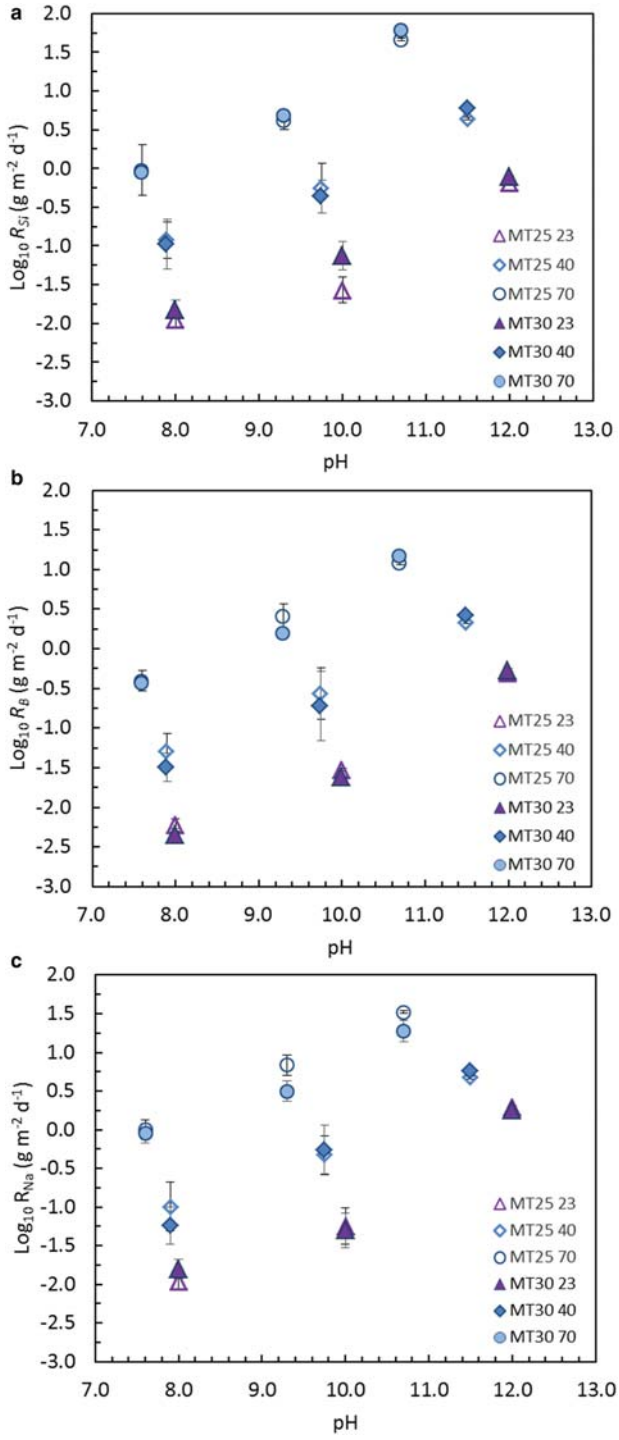

FIG. 3. Log_{10} normalized dissolution rate (R_i, g m^{-2} d^{-1}) as a function of temperature- (23, 40 and 70°C) corrected pH for: (*a*) Si; (*b*) B; and (*c*) Na, released from MT25 and MT30 blend simulated waste glasses.

TABLE 5. Calculated pH power-law coefficient (η) and correlation coefficient (R^2) for MT25 and MT30 blend simulated waste glass, derived from regression analysis based on the steady-state release of Si, B and Na, shown in Fig. 3.

Temperature (°C)	η_{Si}	R^2_{Si}	η_B	R^2_B	η_{Na}	R^2_{Na}
MT25						
23	0.44 ± 0.02	0.97	0.35 ± 0.02	0.99	0.56 ± 0.03	0.96
40	0.44 ± 0.02	0.99	0.45 ± 0.02	0.99	0.46 ± 0.02	0.98
70	0.49 ± 0.02	0.96	0.33 ± 0.02	0.94	0.58 ± 0.03	0.99
MT30						
23	0.42 ± 0.02	0.99	0.52 ± 0.03	0.99	0.51 ± 0.03	0.92
40	0.39 ± 0.02	0.97	0.58 ± 0.03	0.99	0.53 ± 0.03	0.98
70	0.40 ± 0.02	0.99	0.36 ± 0.02	1.00	0.42 ± 0.02	0.99

was not possible to make a comparison of the k_0 values reported here with those resulting from the SPFT investigation of Magnox glass by Abraitis *et al.* (2000*b*,*c*) or with French simulant glasses as the values were not reported.

Effect of waste loading on dissolution rate

The two glass blend compositions investigated in this study contained 25 wt.% and 30 wt.% loadings of Magnox–ThORP blended waste, respectively, with compositions given in Table 1. The forward rates of Si, B and Na dissolution were not found to be very sensitive to the composition, defined by the waste loading. Table 3 shows that the ΔR_i for all elements were more or less within error, except for normalized rates at pH(23°C) = 12.0 at 70°C for Si, B and Na; under these particular conditions there was no clear trend observed to determine whether one glass demonstrated greater dissolution rates than the other; e.g. R_{Si} of MT30 was ~1.3 times greater than that of MT25 but the R_{Na} of MT25 was a factor of ~1.8 times greater than that of MT30. Furthermore, the ΔEa_i for each glass was similar, within error (Table 4), and the power law coefficients (η) were of the same order (Table 5). The intrinsic rate constants (k_0) for each glass differed slightly, though both glasses demonstrated an increase in k_0 with increasing temperature. Further investigation to confirm these observations and their mechanistic origin are required.

It may be concluded that increasing the waste loading by 5 wt.% did not appear to have any measurable effect on the initial dissolution rate, within error. The compositions of the two glasses investigated in the present study represent somewhat subtle changes in glass composition (Table 1); previous studies have shown that dramatically

TABLE 6. Calculated rate constants (k_0) for MT25 and MT30 blend simulated waste glass, derived from regression analysis based on the steady-state release of Si, B and Na, shown in Fig. 3.

Temperature (°C)	k_{Si}	k_B	k_{Na}
MT25			
23	$(2.84 \pm 0.31) \times 10^{-6}$	$(9.77 \pm 0.11) \times 10^{-7}$	$(2.46 \pm 0.27) \times 10^{-7}$
40	$(3.93 \pm 0.43) \times 10^{-5}$	$(1.25 \pm 0.14) \times 10^{-5}$	$(1.93 \pm 0.21) \times 10^{-5}$
70	$(4.68 \pm 0.52) \times 10^{-4}$	$(1.33 \pm 0.15) \times 10^{-3}$	$(1.93 \pm 0.21) \times 10^{-4}$
MT30			
23	$(5.02 \pm 0.55) \times 10^{-6}$	$(3.38 \pm 0.37) \times 10^{-7}$	$(8.04 \pm 0.88) \times 10^{-7}$
40	$(1.21 \pm 0.13) \times 10^{-5}$	$(1.70 \pm 0.19) \times 10^{-6}$	$(3.42 \pm 0.38) \times 10^{-6}$
70	$(8.25 \pm 0.91) \times 10^{-4}$	$(6.46 \pm 0.71) \times 10^{-4}$	$(4.94 \pm 0.54) \times 10^{-4}$

altering the glass composition and Si local structure did not have a measurable effect on the dissolution rate (Icenhower *et al.*, 2008; Pierce *et al.*, 2010) and therefore it is unlikely that the small changes in composition between the two glass blends investigated here would necessarily be expected to give rise to a significant difference in the dissolution rate. Nevertheless, positive demonstration of the sensitivity of the forward dissolution rate to composition within the extended product envelope currently under manufacture should be considered a useful contribution to underpinning the disposability of these products. Prediction of how long-term glass durability may be affected by the addition of greater waste loadings must be undertaken with caution; increasing the mol.% of oxide elements such as Al, Zn and Zr has been shown to increase initial durability due to their role as a glass network former (Della Mea *et al.*, 1986; Cassingham *et al.*, 2011; Connelly *et al.*, 2011; Gin *et al.*, 2012; Zhang *et al.*, 2015). While increasing the loading of waste will lead to an increase in both Al and Zr, their effects on long-term glass durability is not yet well understood.

Conclusions

We report the first comprehensive study of the dissolution kinetics of simulant UK Magnox–ThORP blended HLW glasses over a range of temperatures and alkaline pH regimes, including an investigation of the effect of altering glass composition on dissolution rate. The forward rate of dissolution for MT25 and MT30 blend glasses was found to be temperature and pH dependent, and results suggested that dissolution was a surface-controlled process, limited by the rupture of Si–O bonds and detachment of Si from the glass surface. This process was influenced by the high solubility of silica at high pH, which resulted in elevated dissolution rates at the highest pH values. The addition of 5 wt.% waste to the glass composition had a negligible effect on the dissolution kinetics in the forward rate, probably because of the minimal changes in glass composition and structure through such an addition. This is consistent with the observation that the forward rate of dissolution, based on B release, was in agreement with that previously derived for pure Magnox glass under dilute conditions. In contrast, the dissolution rates found did not agree with those reported in the literature for Magnox and Magnox–ThORP blend glasses due to the experimental variability of the static methodologies employed. These data highlight the importance of using flow-through methodologies to determine the kinetic parameters (η, k_0 and E_a) for UK vitrified HLW that can be applied to the derivation of the source term used in post-closure safety assessments for geological disposal of HLW glass. Extended SPFT experiments at acidic to neutral conditions will probably be beneficial to further understanding the Magnox–THORP blend glass dissolution, as will further long-term dissolution studies of these materials under a variety of conditions relevant to geological disposal environments.

Acknowledgements

This work was funded in full by EPSRC under grant EP/F055412/1: Decommissioning Immobilisation and Management of Nuclear Wastes for Disposal (DIAMOND). NJC is grateful to collaborators at PNNL, especially Dr J. Vienna, Dr D. Wellman and E. Cordova and also to Dr Paul Bingham for useful discussions. CLC is grateful to The University of Sheffield for the award of a Vice Chancellor's Fellowship and DJB acknowledges the EPSRC Nuclear FiRST Doctoral Training Centre for the provision of a studentship under grant EP/G037140/1. NCH is grateful to the Royal Academy of Engineering and the Nuclear Decommissioning Authority for funding.

References

Abraitis, P.K., Livens, F.R., Monteith, J.E., Small, J.E., Trivedi, D.P., Vaughan, D.J. and Wogelius, R.A. (2000*a*) The kinetics and mechanisms of simulated British Magnox waste glass dissolution as a function of pH, silicic acid activity and time in low-temperature aqueous systems. *Applied Geochemistry*, **15**, 1399–1416.

Abraitis, P.K., McGrail, B.P., Trivedi, D.P., Livens, F.R. and Vaughan, D.J. (2000*b*) Single-pass flow-through experiments on a simulated glass in alkaline media at 40°C. I. Experiments conducted at variable solution flow rate to glass surface area. *Journal of Nuclear Materials*, **280**, 196–205.

Abraitis, P.K., McGrail, B.P., Trivedi, D.P., Livens, F.R. and Vaughan, D.J. (2000*c*) Single-pass flow-through experiments on a simulated glass in alkaline media at 40°C. II. Experiments conducted with buffer solutions containing controlled quantities of Si and Al. *Journal of Nuclear Materials*, **280**, 206–215.

ASTM (1994) *Standard Test Methods for determining the chemical durability of nuclear waste glasses: The Product Consistency Test (PCT)*. ASTM C1285–94, Annual Book of ASTM Standards, Philadelphia, USA.

Brady, P.V. and House, W.A. (1996) Surface-controlled dissolution and growth of minerals. Pp. 225–306 in: *Physics and Chemistry of Mineral Surfaces* (P.V. Brady, editor). CRC Press, New York.

Cassingham, N.J., Stennett, M.C., Bingham, P.A. and Hyatt, N.C. (2011) The structural role of Zn in nuclear waste glasses. *International Journal of Applied Glass Science*, **2**, 343–353.

Corkhill, C.L., Cassingham, N.J., Heath, P.G. and Hyatt, N.C. (2013) Dissolution of UK high-level waste glass under simulated hyperalkaline conditions of a co-located geological disposal facility. *International Journal of Applied Glass Science*, **4**, 341–356.

Connelly, A.J., Hyatt, N.C., Travis, K.P., Hand, R.J., Maddrell, E.R. and Short, R.J. (2011) The structural role of Zr within alkali borosilicate glasses for nuclear waste immobilisation. *Journal of Non-Crystalline Solids*, **357**, 1647–1656.

Curti, E., Crovisier, J.L., Morvan, G., and Karpoff, A.M. (2006) Long-term corrosion of two nuclear waste reference glasses (MW and SON68): A kinetic and mineral alteration study. *Applied Geochemistry*, **21**, 1152–1168.

Della Mea, G., Gasparatto, A., Bettinelli, M., Montenero, A. and Scaglioni, R. (1986) Chemical durability of zinc-containing glasses. *Journal of Non-Crystalline Solids*, **84**, 443–451.

Dove, P.M. (1994) The dissolution kinetics of amorphous silica into sodium chloride solutions: effects of temperature and ionic strength. *American Journal of Science*, **294**, 665–712.

Gin, S., Beaudoux, X., Angeli, F., Jegou, C. and Godon, N. (2012) Effect of composition on the short-term and long-term dissolution rates of ten borosilicate glasses of increasing complexity from 3 to 30 oxides. *Journal of Non-Crystalline Solids*, **358**, 2559–2570.

Gin, S., Abdelouas, A., Criscenti, L.J., Ebert, W.L., Ferrand, K., Geisler, T., Harrison, M.T., Inagaki, Y., Mitsui, S., Mueller, K.T., Marra, J.C., Pantano, C.G., Pierce, E.M., Ryan, J.V., Schofield, J.M., Steefel, C.I and Vienna, J.D. (2013*a*) An international initiative on long-term behavior of high-level nuclear waste glass. *Materials Today*, **16**, 243–248.

Gin, S., Frugier, P., Jollivet, P., Bruguier, F. and Curti, E. (2013*b*) New insight into the residual rate of borosilicate glasses: Effect of s/v and glass composition. *International Journal of Applied Glass Science*, **4**, 371–382.

Harrison, M.T., Steele, C.J. and Riley, A.D. (2012) The effect on long term aqueous durability of variations in the composition of UK vitrified HLW product. *Glass Technology: European Journal of Glass Science and Technology A*, **53**, 211–216.

Hyatt, N.C., Taylor, K.J., Gibb, F.G., F. and Lee, W.E. (2004) Crystallisation of Magnox waste glass under conditions of very high temperature, very deep, geological disposal. *Glass Technology*, **45**, 68–70.

Icenhower, J.P. and Dove, P.M. (2000) The dissolution kinetics of amorphous silica in sodium chloride solutions: effects of temperature and ionic strength. *Geochimica et Cosmochimica Acta*, **64**, 4193–4203.

Icenhower, J.P. and Steefel, C.I. (2013) Experimentally determined dissolution kinetics of SON68 glass at 90°C over a silica saturation interval: Evidence against a linear rate law. *Journal of Nuclear Materials*, **439**, 137–147.

Icenhower, J.P., Strachan, D.M., McGrail, B.P., Scheele, R.D., Rodriguez, E.A., Steele, J.L. and Legore, V.L. (2006) Dissolution kinetics of pyrochlore ceramics for the disposition of plutonium. *American Mineralogist*, **91**, 39–53.

Icenhower, J.P., McGrail, B.P., Shaw, W.J., Pierce, E.M., Nachimuthu, P., Shuh, D.K., Rodriguez, E.A. and Steele, J.L. (2008) Experimentally determined dissolution kinetics of Na-rich borosilicate glass at far from equilibrium conditions: Implications for Transition State Theory. *Geochimica et Cosmochimica Acta*, **72**, 2767–2788.

Jollivet, P., Gin, S. and Schumacher, S. (2012) Forward dissolution rate of silicate glasses of nuclear interest in clay-equilibrated groundwater. *Chemical Geology*, **330–331**, 207–217.

Lasaga, A.C. (1981) Transition state theory. Pp. 135–168 in: *Kinetics of Geochemical Processes* (A.C. Lasaga and R.J. Kirkpatrick, editors). Reviews in Mineralogy, **8**, Mineralogical Society of America, Washington DC.

Lasaga, A.C. (1995) Fundamental approaches in describing mineral dissolution and weathering rates. Pp. 23–86 in: *Chemical Weathering Rates of Silicate Minerals* (A.F. White and S.L. Brantley, editors). Reviews in Mineralogy, **31**, Mineralogical Society of America, Washington DC.

Marsal, F., De Windt, L. and Pellegrini, D. (2007) *Modelling of long term geochemical evolution of the bentonite buffer of KBS-3 repository.* Institute de Radioprotection et de Sûreté Nucléaire, Report DSU/SSIAS number 3.

Material Characterisation Centre (MCC) (1981) *Nuclear Waste Materials Handbook,* DOE/TIC 11400, Pacific Northwest Laboratory, Richmond, Washington, USA.

McGrail, B.P. and Peeler, D.K. (1995) *Evaluation of the single-pass flow-through test to support a low-activity waste specification.* PNL-10746, Pacific Northwest Laboratory, Richmond, Washington, USA.

McGrail, B.P., Ebert, W.L., Bakel, A.J. and Peeler, D.K. (1997) Measurement of kinetic rate law parameters on a Na-Ca-Al borosilicate glass for low-activity waste. *Journal of Nuclear Materials*, **249**, 175–189.

Nuclear Decommissioning Authority (2014) *2013 UK Radioactive Waste Inventory: Waste Quantities from all Sources*. NDA Report NDA/ST/STY(14)0010, February 2014.

Pierce, E.M., Icenhower, J.P., Serne, R.J. and Catalano, J. (2005) Experimental determination of UO_2(cr) dissolution kinetics: effects of solution saturation state and pH. *Journal of Nuclear Materials*, **345**, 206–218.

Pierce, E.M., Rodriguez, E.A., Calligan, L.J., Shaw, W.J. and McGrail, B.P. (2008) An experimental study of the dissolution rates of simulated aluminoborosilicate waste glasses as a function of pH and temperature under dilute conditions. *Applied Geochemistry*, **223**, 2559–2573.

Pierce, E.M., Reed, L.R., Shaw, W.J., McGrail, B.P., Icenhower, J.P., Windisch, C.F., Cordova, E.A. and Borady, J. (2010) Experimental determination of the effect of the ratio of B/Al on glass dissolution along the nepheline ($NaAlSiO_4$) – malinkoite ($NaBSiO_4$) join. *Geochimica et Cosmochimica Acta*, **74**, 2634–2654.

Utton, C.A., Swanton, S.W., Schofield, J., Hand, R.J., Clacher, A. and Hyatt, N.C. (2012) Chemical durability of vitrified wasteforms: effects of pH and solution composition. *Mineralogical Magazine*, **76**, 2919–2930.

Vernaz, E. and Dussossoy, L.J. (1992) Current state of knowledge of nuclear waste glass corrosion mechanisms: the case of R7T7 glass. *Applied Geochemistry*, **1**, 13–22.

Wellman, D.M., Icenhower, J.P., Gamerdinger, A.P. and Forrester, S.W. (2006) Effects of pH, temperature and aqueous organic material on the dissolution kinetics of meta-autunite materials, $(Na,Ca)_{2-1}[(UO_2)(PO_4)]_2{\cdot}3H_2O$. *American Mineralogist*, **91**, 143–158.

Wolff-Boenisch, D., Gislason, S.R., Oelkers, E.H. and Putnis, C. (2004) The dissolution rates of natural glasses as a function of their composition at pH 4 and 10.6, and temperatures from 25 to 74°C. *Geochimica et Cosmochimica Acta*, **68**, 4843–4858.

Zapol, P., He, H., Kwon, K.D. and Crisenti, L.J. (2013) First-principles study of hydrolysis reaction barriers in a sodium borosilicate glass. *International Journal of Applied Glass Science*, **4**, 395–407.

Zhang, H., Corkhill, C.L., Heath, P.G., Hand, R.J., Stennett, M.C. and Hyatt, N.C. (2015) Effect of Zn- and Ca-oxides on the structure and chemical durability of simulant alkali borosilicate glasses for immobilisation of UK high level wastes. *Journal of Nuclear Materials*, **462**, 321–328.